Atmos. Meas. Tech. Discuss., 6, 4087–4121, 2013
www.atmos-meas-tech-discuss.net/6/4087/2013/
doi:10.5194/amtd-6-4087-2013

Atmospheric Measurement Techniques Discussions
Open Access

Towards an automatic Lidar cirrus cloud retrieval for climate studies

E. G. Larroza[1], W. M. Nakaema[1], R. Bourayou[1], C. Hoareau[2], E. Landulfo[1], and P. Keckhut[3]

[1]CLA, IPEN/CNEN-SP, Center for Lasers and Apllications, Av. Prof. Lineu Prestes, 2242 São Paulo-SP-Brazil, 05508-000, Brazil
[2]LMD-IPSL, EcolePolytechnique, Route de Saclay, 91128 PalaiseauCedex, France
[3]LATMOS-IPSL, Univesité de Versaille Saint-Quentin (bureau 1323) 11, boulevard d'Alembert, 78280 Guyancourt, France

Received: 26 March 2013 – Accepted: 8 April 2013 – Published: 30 April 2013

Correspondence to: E. G. Larroza (elarroza.ipen@gmail.com) and
P. Keckhut (keckhut@latmos.ipsl.fr)

Published by Copernicus Publications on behalf of the European Geosciences Union.

Abstract

In the present study, a methodology to calculate lidar ratios for distinct cirrus clouds has been implemented for a site located in the Southern Hemisphere. The cirrus cloud lidar data processing has been developed to consider a large cloud variability with the final aim of cirrus cloud monitoring through a robust retrieval process. Among the many features lidar systems can extract for cirrus detection, we highlight: cloud geometrical information and extinction-to-backscatter ratio (also called lidar ratio – LR). LR's can, in general, provide important information on cirrus cloud microphysics due to the presence of ice crystals and their properties such as shape, size, composition and orientation of particles and their effect on LR values. Conditions for LR calculations and their resulting uncertainty have been improved as their analysis requires identifying cirrus cloud stationary periods through the use of a specific statistical approach well-established in the literature and employed here with good results, allowing for the study of specific cases with multi-layer cirrus cloud occurrence. The results from the measurements taken in the region of the Metropolitan City of São Paulo – MSP have been used to implement and test the methodology developed herein. In addition to the geometrical parameters extracted, improved values of LR's were calculated and showed significantly different values for the different layers inspected, varying between 19 ± 01 sr and 74 ± 13 sr. This large value interval allowed us to indirectly verify the presence of different ice crystal sizes and shapes and those associated with different air mass sources for the cirrus cloud formation.

1 Introduction

Cirrus clouds have a complex variety of impacts on climate (Liou, 1986) due to their influence on both earth's incoming and outgoing solar radiation, with their variable radiative and optical properties affecting both the cooling and heating of the earth's atmosphere (Ramanathan and Collins, 1991). Even their topology in the atmosphere

AMTD
6, 4087–4121, 2013

shows an interesting pattern which has a direct impact in the presence of ice crystals of different shapes and sizes (Takano and Liou, 1995; Hallet et al., 2002; Heymsfield and Mcfarquhar, 2002; Nazaryan et al., 2008; Mioche et al., 2010) and in the presence of liquid water at temperatures well below freezing (Hallett et al., 2002; Dodion et al., 2008). Their abundance in the atmosphere at any time can span (on average) from 30 % over the entire globe to up to 70 % over the Tropics (Wang et al., 1996; Nazaryan et al., 2008; Dupont et al., 2010). Additionally, cirrus cloud observation has become much more elusive since it was discovered that a considerable fraction of the clouds are relatively optically thin (in the visible spectrum – Sassen et al., 2008).

Facing this large diversity of characteristics that, currently, are virtually impossible to measure with a single instrument, one must assume that clouds that form in similar conditions and involving the same physical processes as crystals exhibit crystal-like characteristics. However, cirrus cloud occurrence, their simulation by numerical models, and their effects on climate are known to be different depending on their causes of formation. Advances in modeling capability to predict climate change require improved representations of cloud processes in models, as well as a reduction of uncertainties in parameterizations of cloud-radiation interaction (Nazaryan et al., 2008). For these reasons, it is important to identify different classes of cirrus clouds based on the processes involved. Sassen and Cho (1992), in order to separate cirrus clouds into visible and sub-visual cirrus clouds, proposed a threshold for their optical depth of 0.03. While optical depth is a critical parameter to describe clouds, many other characteristics are important for radiative issues such as crystal form, size distribution, composition, etc. Cirrus cloud characteristics, such as their composition, particle, density, size, and form, vary with altitude depending on formation processes (Dupont et al., 2010). Knowing the cloud particle density distribution with altitude is essential for understanding the radiative balance between the greenhouse (terrestrial infrared energy) and albedo effects (solar visible). Cirrus cloud formation is associated with upwelling motions, either due to frontogenesis or convection, and is also strongly driven by horizontal water vapor transport over a wide range of scales, from local to continental, due to isentropic

AMTD
6, 4087–4121, 2013

advection (Fueglistaler et al., 2004; Keckhut et al., 2005; Montoux et al., 2009), including phase changes. Also, cyclones and airplane contrails provide conditions that generate cirrus clouds with unique characteristics. These processes lead to significant vertical and time heterogeneities that may also have a strong impact on the radiative balance. Therefore, the parameterization of high clouds in climate models needs to properly assess the temporal and spatial distribution of its properties (Ringer and Allan, 2004; Li et al., 2005; Nazaryan et al., 2008).

Satellite data cover large areas of the globe, but measurements from satellite radiance are difficult to use to study cirrus clouds that can occur as part of multilayered cloud system and are characteristically optically thin. Although measurements from CloudSat and CALIPSO (Cloud Sat/Cloud-aerosol Lidar and Infrared Pathfinder Satellite Observations), which support a cloud radar and polarization lidar, respectively, are able to identify and accurately measure this category of clouds (Sassen et al., 2008), they do not completely satisfy the need to track the cirrus coverage over the entire globe.

Due to a limited number of vertically and temporally high-resolution measurements of microphysical properties, especially in the tropical/subtropical region of South America, an accurate determination of the radiative forcing of cirrus clouds is difficult to assess. Measurements with a high vertical and temporal resolution can only be achieved with radar and lidar (Seifert et al., 2007). However, their characterization is problematic as such clouds are ubiquitous (Liou, 1986) and their bulk microphysical properties highly variable (Heymsfield, 1972). This variability is transferred during the time-series measurements of backscattering coefficients derived from lidar signals. Nonetheless, ground-based lidar investigations provide useful information that can link macro-physical, optical, and micro-physical properties of cirrus clouds with synoptic and radiative processes (Sassen and Campbell, 2001; Sassen and Benson, 2001; Sassen and Comstock, 2001; Sassen et al., 2003, 2007). Some investigations about the vertical distribution of cirrus clouds have revealed an identification of clusters that can be associated with specific formation processes (Keckhut et al., 2006; Hoareau et

AMTD
6, 4087–4121, 2013

al., 2012). Single wavelength lidar can provide us with an important parameter called the extinction to backscattering ratio, also named the lidar ratio (LR). This ratio depends on many characteristics of the particles including their shape, size distribution, and refractive index, (Ansmann et al., 1992; Ackermann, 1998; Ansmann, 2002; Chen et al., 2002; Barnaba and Gobbi, 2004; Cadet et al., 2005; Josset et al., 2012) and can give us a hint about the ice-crystal characteristics (Sassen et al., 1989; Ansmann, 2002; Petty et al., 2006). In addition, the lidar ratio is required to retrieve an accurate scattering ratio through the determination of the extinction coefficient $\alpha(z)$ from the signal retrievals (Petty et al., 2006). Accurate estimates depend on many factors such as optical depth ($\tau_{cir} < 0.03$ for subvisible clouds; Sassen and Cho, 1992; Sassen et al., 2008), variable multi-scattering effects inside cloud layers, and lidar signals mainly driven by the statistical noise level.

To obtain a reliable statistical data set of vertical distribution characteristics and optical properties for different categories of cirrus clouds, a large number of photons need to be collected and lidar signals need to be averaged. In addition, due to the high spatio-temporal geophysical variability, the selected periods need to include consistent cloud information and careful investigations are required to select cloud scenes. Here, a methodology is proposed to provide pertinent and more robust information about cloud altitude, thickness, optical depth (τ_{cir}) and LR in a so-called stationary period (Lanzante, 1996) when clouds could exhibit similar micro- and macro-physical properties and when molecular scattering can be detected above clouds to perform accurate retrievals (Morille et al., 2007). Multi-layer cirrus clouds are also an issue when one wants to derive cloud thickness or optical depths. In these cases, it is a challenge to derive their individual optical properties if layers exhibit overlap such that no pure Rayleigh scattering between the layers can be observed. Selected lidar data are used to retrieve characteristics when they are feasible to provide improved cloud characteristic retrieval that will help to obtain consistent cirrus cloud families according to their formation. Such databases will be useful to investigate if such processes are properly included in numerical models leading to a proper climate radiation budget (Josset et

AMTD
6, 4087–4121, 2013

al., 2012). Lidar measurements from São Paulo provide a good opportunity to understanding their morphology and effects on the regional basis. While the methodology is based on these lidar data sets, the methodology and criteria are universal.

The manuscript is organized as follow: Sect. 2 gives a brief description of the lidar system used. In Sect. 3 the methodology is described, providing the full cirrus cloud macro-physical and optical properties derived from these lidar observations for one specific date: 11 June 2007. It includes data selection criteria and multiple scattering effects corrections of the derived optical properties – τ_{cir} and LR. The overall uncertainties in our methodology are discussed in Sect. 4. The results are discussed in Sect. 5, followed by the conclusion in Sect. 6.

2 Description of the lidar and location

A ground-based elastic backscatter lidar system, located in the metropolitan city of São Paulo (23°33′ S, 46°44′ W) in Brazil, has been operated in the Laboratory of Environmental Laser Applications at the Center for Lasers and Applications (CLA) at the Instituto de Pesquisas Energéticas e Nucleares (IPEN) since 2001 (Landulfo et al., 2003). Initially implemented for the measurement of aerosols and atmospheric boundary layers, the systematic cirrus cloud measurements began in 2004 and remain ongoing.

The lidar system is a single-wavelength backscatter system pointing vertically to the zenith and operating in the coaxial mode. The light source is based on a commercial Nd : YAG laser (Brilliant by Quantel SA) operating at the second harmonic frequency (SHF), namely at 532 nm for cirrus detection, with a fixed repetition rate of 20 Hz. The average emitted power can be selected up to values as high as 3.3 W. The emitted laser pulses have a divergence smaller than 0.5 mrad. A 30 cm diameter telescope (focal length $f = 1.3$ m) is used to collect the backscattered laser light. The temporal resolution of measurements is ∼2 min and the vertical resolution is 15 m. The data acquisition was mostly done in dual-mode, this means both analog and photo-counting. In general, for detection of cirrus occurrence, SR calculations, AOD estimation, the

AMTD
6, 4087–4121, 2013

analog signal was determinant. The photo-counting mode was employed specially to define a threshold factor to accurately define base and top.

In this study, we focus the results and discussion on lidar measurements from São Paulo taken on 11 July 2007 (Fig. 1), to illustrate the methodology because this case provided the most challenging issues.

The region is considered to have a humid subtropical climate. During the winter (when the measurements were carried out), the temperature usually ranges between 11 °C and 23 °C. The average precipitation registered in this period is about 47 mm, representing a dry season for the Southeast region in Brazil and the weather predominantly consists of relatively cool and clean sky days, but eventually with frontal system passages. Also, inversion events are most frequent during this period, resulting in trapped pollution close to the ground in such a way that the boundary layer does not exceed 1.5 km (as we can see in the Fig. 1). For these reasons, most of the lidar measurements are carried out during the wintertime.

The origin of the detected cirrus can be associated with several phenomena such as deep-convection cumulus clouds and air mass injection provided from the inter-tropical convergence zone (ITCZ) several days before the detection.

In order to determine the origin of air masses that have been probed by the lidar, 72 h backward trajectories were generated using the HYSPLIT model (Draxler and Rolph, 2013). Figure 2 shows a backward trajectory ending on 11 June 2007 at 15:00 UTC, corresponding to the period when two distinct cirrus layers are observed (Fig. 1). The respective trajectories are quite robust over several hours and reveal that both layers observed by the lidar correspond in fact to two distinct cirrus clouds having different origins. Consequently, cirrus cloud climatology should take into account multi-layer cases that are not always due to a vertical structure of the same cloud but could be due to different air masses observed at different altitudes, thus having potentially different optical properties. The lower trajectory in the Fig. 2 (red lines) corresponds to a layer of cirrus clouds observed approximately between 14:00 and 16:00 UTC at 9 km (Fig. 1). The back trajectory shows that the air mass has its origin mostly from the central western

AMTD
6, 4087–4121, 2013

part of Brazil. On the other hand, the higher trajectory (blue line) corresponds to the cirrus clouds at an altitude of 11 km, with the air mass coming from the South Pacific Ocean.

3 Description of the methodology

Our goal was to retrieve accurate information on cirrus cloud locations and optical properties (the LR and the τ_{cir}) when these quantities were related to both geometrical and microphysical properties. An iterative process was used to treat our single-wavelength measurements as described in Goldfarb et al. (2001). However, due to the optical retrieval, this iterative process was performed on profiles averaged over time periods longer than the initial resolution (2 min). Due to the high variability in the measured lidar signals, the averaging processes needed to be performed during periods when the cloud features could be considered stationary. These periods were identified following the approach described by Lanzante et al. (1996), and to consider (temporally and spatially) stationary cloud characteristics, such periods were assumed to be representative of unchanged micro- and macro-physical cloud properties. For some periods, lidar signals were not accurate enough or selected measurement windows corresponded to transition periods when stationary conditions were not satisfied.

When two cloud layers were observed from the lidar signals and assumed to have different origins, the method was more complex and signal enhancement was considered for two independent layers. In these cases, optical properties (LR) were retrieved only if pure Rayleigh scattering could be detected between both layers.

The detail of the procedure will be presented in the next sections and was summed up in Fig. 7 as a flow chart.

AMTD
6, 4087–4121, 2013

3.1 Selection of the cirrus clouds and determination of stationary periods

The ratio between measured molecular and aerosol scattering $\beta^{\text{meas}}_{\text{Rayleigh}} + \beta^{\text{meas}}_{\text{Mie}}$, and the theoretical Rayleigh backscatter coefficient $\beta^{\text{th}}_{\text{Rayleigh}}$ forms the scattering ratio (SR) profiles.

$$\text{SR} = \frac{\beta^{\text{meas}}_{\text{Rayleigh}} + \beta^{\text{meas}}_{\text{Mie}}}{\beta^{\text{th}}_{\text{Rayleigh}}} \quad (1)$$

The signal consists of an individual lidar measurement obtained during a time-average of the return signals, typically over two minutes (initial time resolution), corrected for the background offset and the altitude-squared dependence. This lidar signal corresponds to molecular and aerosol scattering uncorrected for the extinction. The molecular backscattering $\beta^{\text{th}}_{\text{Rayleigh}}$ can be estimated from a dry air density profile, retrieved from the conventional radiosonde observation profile (Bucholtz, 1995). Only the lidar profiles containing a cirrus cloud signal were retained. Signals displaying a cloud base below 7.5 km were discarded (Das et al., 2009 used above 8 km), as well as cirrus clouds having a base temperature, as derived from radiosonde observations, above −20 °C. Below this temperature, clouds particles present a poly-crystaline patterns which can be used to differentiate between ice clouds and water clouds (Heymsfield and Platt, 1984).

In an atmosphere free of aerosols, the SR should be unity by definition. However, Eq. (1) defines the SR as the ratio of experimental and modeled quantities; the denominator is as mentioned before, calculated from the profiles of thermodynamic quantities measured by radiosondes, or simply approximated using an exponential fit of the lidar-measured profile in an altitude range where a free atmosphere is assumed. For these reasons, SR in the free atmosphere may deviate from unity locally. Despite extinction being small for cirrus clouds, the SR obtained with this method is what we can called an "apparent lidar scattering ratio", SR_{app}, (Eq. 2) while extinction is not taken into account. Our period-averaged SR_{app} profiles were normalized by a factor k in order to

AMTD
6, 4087–4121, 2013

assess a mean value of unity in the typical range of altitude between 3 km and 7.5 km, where we assume a purely molecular atmosphere:

$$\mathrm{SR_{app}} = k \times \mathrm{SR} = \frac{\sum_{z=3.0\,\mathrm{km}}^{z=7.5\,\mathrm{km}} \beta^{\mathrm{th}}_{\mathrm{Rayleigh}}(z)}{\sum_{z=3.0\,\mathrm{km}}^{z=7.5\,\mathrm{km}} \left(\beta^{\mathrm{meas}}_{\mathrm{Rayleigh}}(z) + \beta^{\mathrm{meas}}_{\mathrm{Mie}}(z)\right)} \times \mathrm{SR} \quad (2)$$

For our SR profiles, a typical normalization factor was found as $k = 1.011 \pm 0.004$.

The return signal associated with cirrus clouds exhibits a sharp enhancement of up to 100 times the molecular scattering at the same altitude (Seifert et al., 2007). Thus, the edges of the cirrus clouds are characterized by both a steep increase and a steep decrease. The cloud base and top altitudes, respectively z_{base} and z_{top}, can be derived using the following criterion based in Goldfarb et al. (2001).

SR > a threshold value t_{SR}, defined as:

$$t_{\mathrm{SR}} = 1 + 3 \times (\Delta\mathrm{SR}) \quad (3)$$

where the standard deviation ΔSR is, according to Keckhut (2006), calculated as

$$\frac{\Delta\mathrm{SR}}{\mathrm{SR}} = \frac{\sqrt{N}}{N - B} = \frac{\sqrt{N_{\mathrm{p}} + B}}{N_{\mathrm{p}}}, \quad (4)$$

with N being a combination of the backscattered number of photons N_{p} and the parasite signal from the sky background B that corresponds to the average number of photons in the last 10 km of the measured signal.

The factor 3 is chosen for the threshold once it corresponds to a significant cloud detection at 99 % over the SR profile (Goldfarb et al., 2001; Cadet et al., 2005; Keckhut et al., 2006). The procedure mentioned above is illustrated in Fig. 3 with the blue line representing the respective threshold profile over the SR profile (red line).

The mid-cloud height z_{med} is defined as the geometric center of a cirrus cloud, i.e., the arithmetic mean of z_{base} and z_{top}, and it is directly associated with the corresponding temperature on a radiosonde profile, being denominated $T_{z\mathrm{med}}$ for consistency. The

AMTD
6, 4087–4121, 2013

number of layers was obtained by identifying successive regions where abrupt variations of the signal (as described before) could potentially be associated with cloud base/top.

The individual (noisy) backscattering profiles shall now be grouped according to the above-presented geometrical features of the cloud layers. For stationary atmospheric conditions, the backscattered photons hit the sensor following a stochastic Poisson process, and sampling over long enough periods provide a better statistical estimator of the cirrus cloud physical properties. However, cirrus clouds are composed by complex structures due to wind shears. As the clouds are spatially very inhomogeneous, different types of cirrus clouds (originated by distinct processes or origins) can be present simultaneously in different layers and the morphology of the clouds in the lidar FOV can also vary greatly in one cloud system. As a result, long sampling periods would smear this information and compromise any climatology studies. To better cope with this variability, we used a method that consisted of adjusting the integration time by clustering similar cloud parameters in the acquisition sequence, inspired from the works of Hoareau et al. (2009). To identify discontinuities in cirrus cloud features in the present study, two complementary time series were investigated: the optical depth $\tau_{\mathrm{cir}}(\mathrm{L})$ and geometrical thickness CT (L) of the cirrus layer L. If cloud thickness changed significantly, it was clearly a sign of a fundamental change of the cloud characteristics. Additionally, if only optical characteristics were changing, then the optical depth may have been sensitive to it. The altitude range was restrained to the extreme values of the base and top altitude of the cirrus clouds identified previously (between 8 and 11.5 km in the case presented on Fig. 1).

Approximate values of the optical depth $\tau_{\mathrm{cir}}(\mathrm{L})$of a cirrus layer L were derived from its transmittance TT (L) using the ratio of the apparent lidar SR values above and below the cloud layer, where it is assumed as clear atmosphere with purely molecular scattering (Cadet et al., 2005). This transmittance is defined as:

$$\mathrm{TT(L)} = \frac{\mathrm{SR}_{z>z_{\mathrm{top}}(\mathrm{L})}}{\mathrm{SR}_{z<z_{\mathrm{base}}(\mathrm{L})}} \quad (5)$$

AMTD
6, 4087–4121, 2013

The values in this ratio are mean values over a given altitude range above z_{top} and below z_{base}. In some cases, the region between two layers, say L1 and L2, is very narrow (typically less than 1 km) and possibly suffers cloud overlap and mixing or the influence of residual aerosols. In this case, as there was not enough overhead to draw a reasonable average value, we used the minimum SR value in this range in the calculation. This case is illustrated in the Fig. 4a.

The optical depth $\tau_{cir}(L)$ of the layer L is then calculated from the inferred transmittance using its definition:

$$\tau_{cir}(L) = -0.5 \times (\ln(TT(L))) \quad (6)$$

The geometrical cloud thickness CT (L) is readily calculated as the difference between the values of the top and of base altitudes z_{base} and z_{top}.

Discontinuities in the time series of τ_{cir} and CT were identified using the test of non-stationarity of the series due to a change in the dispersion (variance). The procedure applied was an iterative method designed to research the multiple change-points in arbitrary series values (Lanzante, 1996) and was already applied to a cirrus cloud series (Hoareau et al., 2012); it is based on a non-parametric statistical test (Wilcoxon-Mann-Whitney significance test) followed by an adjustment of the median. This process was reiterated until a significant continuity was found. A refining procedure compared the variation of τ_{cir} and CT and discarded the data intervals where a contrary trend was found. Figure 5 shows an example of the results of this analysis for data acquired on 11 June 2007. Taking into account both criteria, seven periods were identified and episodes of contrary trends (transitions) were marked with an "X" sign.

The scattering ratio profile for each of these periods of stationary cloud properties can be calculated by averaging all of the eligible individual profiles in a given interval. An example for the 11 June 2007 is displayed in Fig. 6. These averaged SR profiles were used to retrieve the other optical cloud characteristics through the values of the RL and the optical depth τ_{cir} associated with each individual cirrus.

AMTD
6, 4087–4121, 2013

3.2 Retrieval of cirrus physical and optical characteristics

To alleviate the under determination of the LR, and aiming at identifying the optical properties, we will now proceed iteratively on the period-averaged SR profiles. For this, our analysis relied on the transmittance method as described in (Young, 1995) and (Chen et al., 2002). The final LR was calculated for each cloud layer through iterative processes updating the τ_{cir} and SR values until the convergence of LR was achieved. The iterative part of the process is displayed in the right panel of Fig. 7.

Transmittance method

An example of a normalized SR profile is displayed in Fig. 4b, where the denominator $\beta^{th}_{Rayleigh}$ of Eq. (1) was fitted to the measured signal in the above-cited 3.0–7.5 km range. Above the first layer of clouds, we observe a slight decrease in the SR values. Due to the attenuation of the laser pulse, the experimental signal (numerator of Eq. 1) decreases while the signal, as predicted from a fit in the free atmosphere under the cloud layer (denominator of Eq. 1), does not take this effect into account. This attenuation is modeled using the transmittance, as we described in Eq. (5). The optical depth $\tau_{cir}(z_L)$ of such a cloud layer L is then given by Eq. (6). We can now perform a correction for the values of the scattering ratio in the cirrus layer, using

$$SR_{corrected}(z_L) = \frac{SR_{app}(z_L)}{e^{-2\tau_{cir}(L)}} \quad (7)$$

where z_L are altitude levels of the cloud layer L. The original scattering ratio is divided by the exponential corresponding to the (two-way) attenuation of the laser pulse after crossing the layer L.

New lidar ratio values $LR(z_L)$ can now be calculated (by the method described by Goldfarb et al., 2001 and also in Cadet et al., 2003) at the locus of the cirrus layers combining the two following equations. The optical depth is defined as the local integral

AMTD
6, 4087–4121, 2013

of the extinction coefficient, $\alpha(z_L)$:

$$\tau_{cir}(L) = \int_{z_{base}(L)}^{z_{top}(L)} \alpha(z_L) dz_L \quad (8)$$

while $\alpha(z_L)$ can be found as the product of LR and the experimental backscattering $\beta^{meas}_{Rayleigh} + \beta^{meas}_{Mie}$ at the considered altitudes z_L:

$$\tau_{cir}(L) = \int_{z_{base}}^{z_{top}} \alpha(z) dz = LR(z_L) \times \sigma_{Rayleigh} \int_{z_{base}}^{z_{top}} n_{air}(z) \times (SR(z) - 1) dz \quad (9)$$

where $\sigma_{Rayleigh}$ is the Rayleigh backscattering cross section, and $n_{air}(z_L)$ is the density of air, as calculated using vertical profiles of temperature and pressure provided by the radiosonde observations[1].

The final LR was recalculated for each cloud layer through iterative processes updating the $\tau_{cirrus}(L)$ and $SR(z_L)$ values through Eq. (4). Uncertainties were calculated simultaneously, taking into account photon noise, SR calibration, and radiosonde uncertainty.

All of the above calculations were repeated until a consistent and non-variation value for $LR(z_L)$ was found between iterations.

As summarized in the flow chart of Fig. 7, for each cirrus layer, we identified the following macro-physical properties: base and top altitudes z_{base} and z_{top}, mid height z_{med}, and cloud thickness CT. Using radiosonde observation profiles, we were also able

[1]To demonstrate the Eq. (9), we start with the definition $SR = (\beta_{Ray} + \beta_{Mie})/\beta_{Ray}$, so $\beta_{Mie} = \beta_{Ray}(SR - 1)$. Inside of the cloud, the Lidar Ratio can be approximated by $LR = \alpha/\beta \approx \alpha/\beta_{Mie}$, once β_{Ray} is negligible for this region compared to β_{Mie}. So $\alpha \approx LR\beta_{Mie} = \beta_{Ray}(SR - 1) = \sigma_{Ray} N_{air}(SR - 1)$.

AMTD
6, 4087–4121, 2013

to derive the associated temperatures $T_{z\text{base}}$, $T_{z\text{top}}$ and $T_{z\text{med}}$. Finally, relevant optical properties, including the optical depth τ_{cir}, transmittance TT, and lidar ratio LR were also retrieved for each cirrus layer with associated uncertainties.

3.3 Multiple scattering effects

Depending on the composition (ice and water), density, and thickness of clouds, multiple scattering can contribute non-negligibly to the lidar signal (Eloranta, 1998). The effective optical depths retrieved by a lidar are overestimated as retarded photons still contribute to the signal (Josset et al., 2012). Several approaches and formalisms have been proposed to correct for this effect (Platt, 1973; Eloranta, 1998; Bissonnette, 2005; Mitrescu, 2005; Giannakaki et al., 2007) and found that multiple scattering is related primarily to the optical depth. We settled for the effective correction factor η on the observed backscatter coefficient as defined by Platt (1973). For a cirrus layer L of a given optical depth $\tau_{\text{cir}}(\text{L})$, $\eta(\text{L})$ can be calculated as (Chen et al., 2002):

$$\eta(\text{L}) = \frac{\tau_{\text{cir}}(\text{L})}{\exp\left(\tau_{\text{cir}}(\text{L})\right) - 1} \tag{10}$$

This formula gives a description of the increase of multiple scattering effects with optical depth. For most of the cirrus layers studied in this work, it was expected that this factor did not exceed 0.6, once the deepest cloud had no more than 0.92 of optical depth (Table 2). Effective values for the optical depth $\tau_{\text{cir}}(\text{L})$ and lidar ratio $\text{LR}\,(z_{\text{L}})$ are given by (Josset et al., 2012):

$$\tau\eta\tau_{\text{eff}}(\text{L}) = (\text{L}) \times_{\text{cir}} (\text{L}) \tag{11}$$

$$\eta\text{LR}_{\text{eff}}(z_{\text{L}}) = (\text{L}) \times \text{LR}(z_{\text{L}}) \tag{12}$$

AMTD
6, 4087–4121, 2013

4 Uncertainty analysis

4.1 Optical depth and lidar ratio uncertainties

Errors in standard LIDAR analyses have already been discussed and demonstrated in Keckhut et al. (2006) and we are following this standard definition of the uncertainty. It is known that the main uncertainty in lidar measurement is directly related to the photon noise. This standard error is proportional to the square of the number of photons received as described by Eq. (4).

Following this formulation allows us to obtain the uncertainties for the transmittance of each layer:

$$\frac{\Delta \mathrm{TT}(z)}{\mathrm{TT}(z)} = \sqrt{\left(\frac{\Delta \mathrm{SR}(z)_1}{\mathrm{SR}(z)_1}\right)^2 + \left(\frac{\Delta \mathrm{SR}(z)_2}{\mathrm{SR}(z)_2}\right)^2} \tag{13}$$

with the indices "1" and "2" indicating, respectively, values below the base and above the top of cloud, i.e, the regions where the Rayleigh signal is predominant and the noise comes exclusively from the photon counting.

Equation (6) allows us to calculate the uncertainty for the optical depth τ_{cir} and can be written as:

$$\Delta\tau_{\mathrm{cir}}(z) = \left[-\ln\left(\mathrm{TT}(z) + \frac{\Delta \mathrm{TT}(z)}{2}\right)\right] - \left[-\ln\left(\mathrm{TT}(z) - \frac{\Delta \mathrm{TT}(z)}{2}\right)\right] \tag{14}$$

Finally, the relative error on the lidar ratio *LR* can be considered the same for the optical depth (due to the linear relation between τ_{cir} and LR on Eq. 9)

$$\delta \mathrm{RL} = \frac{\Delta\tau_{\mathrm{cir}}(z)}{\tau_{\mathrm{cir}}(z)} \tag{15}$$

and the error for LR is given by:

$$\delta\Delta \mathrm{RL} = \mathrm{RL} \times \mathrm{RL} \tag{16}$$

AMTD
6, 4087–4121, 2013

4.2 Correction of uncertainties taking account the multi-scattering effect

The respective corrections should be made for the uncertainties just as the effective values for optical depth and lidar ratio should be determined taking into account the multi-scattering effect. It can be done by using ordinary propagation in error analysis for the Eqs. (10), (11), and (12).

$$\Delta\tau_{\text{eff}}(z) = \sqrt{(\eta(z))^2(\Delta\tau_{\text{cir}}(z))^2 + (\tau_{\text{cir}}(z))^2(\Delta\eta(z))^2} \quad (17)$$

$$\Delta\text{LR}_{\text{eff}}(z) = \sqrt{(\eta(z))^2(\Delta\text{LR}(z))^2 + (\text{LR}(z))^2(\Delta\eta(z))^2} \quad (18)$$

5 Discussion of the cirrus properties obtained

The methodology presented here was applied to the lidar data series acquired on 11 June 2007, with the lidar system localized at the Center for Lasers and Applications/IPEN (metropolitan region of São Paulo, SP, Brazil). Table 1 presents the macrophysical properties and Table 2 the associated optical properties found for the measured cirrus clouds divided into seven periods, as mentioned before. The periods 1–4 correspond to multi-layer clouds and 5–7 to a mono-layer cloud (Fig. 5). For the multi-layer case, the lowest clouds present bases between 7.69 and 8.05 km and tops between 9.01 and 9.56 km, while the highest clouds present bases between 9.79 and 10.09 km and tops between 10.89 and 11.19 km. For the mono-layer clouds, the bases range between 7.51 and 8.73 km and the tops between 10.74 and 10.83 km. This indicates that the distinct and thinner clouds observed for the four initial periods are followed by a single, thicker layer of clouds for the final three periods as can be clearly seen in Fig. 1. Obviously, this behavior has a direct impact on the optical properties of clouds as can be seen in Table 2 where, for instance, the optical depths do not exceed 0.30 (after multi-scattering correction) for the first four periods while for the last three

AMTD
6, 4087–4121, 2013

periods one can find an optical depth of 0.56. At the same time, one can realize the importance of taking into account the multi-scattering process and the respective corrections that can produce differences of up to 39 % between the apparent (τ_{cir_app}) and effective (τ_{cir_eff}) optical depths (period 6).

Cirrus optical depth (τ_{cir}) is a valuable indicator for which category the clouds can be classified. According to Sassen (2002), the clouds appearing during the first four periods can be classified as thin cirrus ($0.03 < \tau_{cir} < 0.30$), while the last three periods are mostly composed of thick cirrus ($0.3 < \tau_{cir} < 3.0$). No subvisible cirrus ($\tau_{cir} < 0.03$) was detected in this case.

Cloud temperature information was obtained from radiosonde balloons, which were launched twice a day at 00:00 UTC and 12:00 UTC near Campo de Marte airport, located approximately 12 km from the MSP-Lidar system. For the present analysis, we considered the data at 12:00 UTC for the respective day when the lidar measurements were carried out. Temperature changes along the lidar measurements are not available and cirrus changes cannot be correlated with short-term temperature changes. While simultaneous temperature an lidar measurements using Raman techniques would be valuable, the information of mean temperature is still important. The temperature in the mid-cloud heights (T_{zmed}) is distributed between −47.2 and −29.9 °C, indicating that the some of these clouds may present mixed-phases as mentioned in Giannakaki et al. (2007), and a possible impact of water clouds should not be completely disregarded. However, information about different phases in clouds is usually obtained using depolarization channels (Chen et al., 2002; Lampert, 2010) that in our case were not available.

The lidar ratio derived from the multi-layer cases reveals good stability for the three first periods: an average value of 25 sr is obtained for the lowest layer, and 38 sr for the upper, indicating different optical characteristics. The fourth period shows a significant change of the LR value for the upper cloud indicating a possible presence of different types of crystals when compared with the three first periods. The last three periods represent the collapse of the two distinct clouds to form a monolayer. This monolayer

AMTD
6, 4087–4121, 2013

presents LR values around 20 sr indicating the appearance of crystals with different shapes and orientations again followed by some phase changes.

Some authors have tried to correlate the respective mid-cloud temperature with lidar ratios, although such a clear dependence is not obvious (Seifert et al., 2010). Whiteman et al. (2004), for example, verified a general trend of an increase in lidar ratios with decreasing temperatures for their observations carried out at the Andros Islands, Bahamas. They found values of about 15–17 ± 10 sr at −30 °C, 22 ± 8 sr at −50 °C, and 28–33 ± 12 sr at temperatures around −70 °C when excluding hurricane-influenced cases. In the same way, lidar observations conducted in Taiwan from August 1999 to July 2000 presented by Chen et al. (2002) showed lidar ratios ≤ 50 sr for 90 % of measurements after multiple-scattering corrections. In the altitude ranges between 12 km (−50 °C) to 15 km (−70 °C), they found lidar ratios of about 35 ± 15 sr. Platt et al. (2002), using the LIRAD method (combined lidar and infrared radiometry measurements – Platt, 1973) for observations acquired during the Maritime Continent Thunderstorm Experiment (MCTEX) close to Australia, retrieved lidar ratios ranging from 42 to 74 sr for temperatures between −45 °C and −70 °C, respectively. Recent analysis using the ocean surface observations from CloudSat radar and data from Cloud Aerosol Lidar with Orthogonal Polarization (CALIOP) on board the Cloud Aerosol Lidar and Infrared Pathfinder Observations (CALIPSO) (Winker et al., 2010), combined in the Synergized Optical Depth of Aerosol (SODA) algorithm, was performed by Josset et al. (2012). They found, for the preliminarily selected data, lidar ratios varying between 30 and 34 sr respectively for the temperature range of −70 °C and −40 °C and also presenting a maximum slightly higher than 34 sr at −50 °C. In our case, the effective lidar ratios (LR_{eff}) do not exceed 35 sr (besides period 4 exhibit a LR value of 69 ± 12 sr) for the early mentioned range of temperature, although no clear dependence between these variables can be established again.

This variability can be related to the different types of cloud studied in different campaigns associated with geographical variations. Although there seems to be a connection between lidar ratio and temperature which could in turn lead to a different ice

AMTD
6, 4087–4121, 2013

nucleation process with distinct optical properties of ice crystals, a thorough analysis that permits a classification of cirrus type and origin or formation mechanisms must follow and is out of the scope of this manuscript.

What is important to stress here is the ability to calculate distinct values of lidar ratios for different cirrus formations in a consistent way with an alternative and robust methodology. The approach inferred here should be implemented in the near future to generate a nine-year (2004–2012) lidar-retrieved cirrus database over São Paulo that will determine the cirrus climatology and establish an operational routine of analysis.

6 Conclusions

We have presented here an alternative and robust method to calculate lidar ratios for distinct cloud layers depending on measurement conditions. The retrieved lidar ratios are shown to be somewhat consistent with those obtained by other authors in different contexts for a given range of (mid-cloud) temperatures. The robustness of this method is based on a detailed previous selection of cirrus occurrence periods and the further application of non-parametric statistics to determine the so-called homogeneous periods. The scatter ratio profiles for such periods produce the necessary cirrus macro-physical and optical parameters. The iterative routine will assure the stability of lidar-obtained ratios as well as their respective optical depths. This last variable also determines, in a simple way, the multiple scattering factor that should be applied to a final estimation of values. Once the effectiveness of this method is verified, future analysis should be applied for a long-term, lidar-measured cirrus database to obtain the climatology of cirrus clouds in the São Paulo region, the first of this type performed in Brazil.

Acknowledgements. This work has been supported by the Conselho Nacional de Desenvolvimento Científico e Tecnológico (CNPq), under the project number 202007/2008-1 and 150760/2012-4, the support of Conselho Nacional de Energia Nuclear – CNEN/Brazil. The

AMTD
6, 4087–4121, 2013

authors thank their colleagues for continuing support and fruitful discussion about the contents of this manuscript.

References

Ackermann, J.: The extinction-to-backscatter ratio of tropospheric aerosol: a numerical study, J. Atmos. Ocean. Tech., 15, 1043–1050, doi:10.1175/1520-0426(1998)015<1043:TETBRO>2.0.CO;2, 1998.

Ansmann, A.: Molecular-Backscatter Lidar Profiling of the Volume-Scattering Coefficient in Cirrus, in: Cirrus, edited by: Lynch, D. K., Sassen, K., Starr, D. O'C. and Stephens, G., Oxford University Press, London, 197–210, 2002.

Ansmann, A., Riebesell, M., Wandinger, U., Weitkamp, C., Voss, E., Lahmann W., and Michaelis, W.: Combined Raman elastic-backscatter LIDAR for vertical profiling of moisture, aerosol extinction, backscatter, and LIDAR ratio, Appl. Phys. B, 55, 18–28, 1992.

Barnaba, F. and Gobbi, G. P.: Modeling the aerosol extinction versus backscatter relationship for lidar applications: maritime and continental conditions, J. Atmos. Ocean. Tech., 21, 428–42, 2004.

Bissonnette, L. C., Roy, G., and Roy, N.: Multiple-scattering-based lidar retrieval: method and results of cloud probings, Appl. Optics, 44, 5565–5581, doi:10.1364/AO.44.005565, 2005.

Bucholtz, A.: Rayleigh-scattering calculations for the terrestrial atmosphere, Appl. Optics, 34, 2765–2773, doi:10.1364/AO.34.002765, 1995.

Cadet, B., Goldfarb, L., Faduilhe, D., Baldy, S., Giraud, V., Keckhut, P., and Rechou, A.: A subtropical cirrus clouds climatology from Reunion Island (21°S, 55° E) lidar data set, Geophys. Res. Lett., 30, 30.1–30.4, 2003.

Cadet, B., Giraud, V., Haeffelin, M., Keckhut, P., Rechou, A., and Baldy, S.: Improved retrievals of the optical properties of cirrus clouds by a combination of lidar methods, Appl. Optics, 44, 1726–1734, 2005.

Chen, W. N., Chiang, C. W., and Nee, J. B.: Lidar ratio and depolarization ratio for cirrus clouds, Appl. Optics, 41, 6470–6476, doi:10.1364/AO.41.006470, 2002.

Das, S. K., Chiang, C. W., and Nee, J. B.: Characteristics of cirrus clouds and its radiative properties based on lidar observation over Chung-Li, Taiwan, Atmos. Res., 93, 723–735, doi:10.1016/j.atmosres.2009.02.008, 2009.

AMTD
6, 4087–4121, 2013

Draxler, R. R. and Rolph, G. D.: HYSPLIT (HYbrid Single-Particle Lagrangian Integrated Trajectory) Model access via NOAA ARL READY Website, available at: http://ready.arl.noaa.gov/HYSPLIT.php (last access: 14 February 2013), NOAA Air Resources Laboratory, Silver Spring, MD, 2013.

Dodion, J., Fussen, D., Vanhellemont, F., Bingen, C., Mateshvili, N., Gilbert, K., Skelton, R., Turnbull, D., Mcleod, S. D., Boone, C. D., Walker, K. A., and Bernath, P. F.: Aerosols and clouds in the upper troposphere–lower stratosphere region detected by GOMOS and ACE: Intercomparison and analysis of the years 2004 and 2005, Adv. Space Res., 42, 1730–1742, doi:10.1016/j.asr.2007.09.027, 2008.

Dupont, J.-C, Haeffelin, M., Morille, Y., Noël, V., Keckhut, P., Winker, D., Comstock, J., Chervet, P., and Roblin, A.: Macrophysical and optical properties of mid-latitude high-altitude clouds from 4 ground-based lidars and collocated CALIOP observations, J. Geophys. Res., 115, D00H24, doi:10.1029/2009JD011943, 2010.

Eloranta, E. W.: Practical model for the calculation of multiply scattered lidar returns, Appl. Optics, 37, 2464–2472, doi:10.1364/AO.37.002464, 1998.

Fueglistaler, S., Wernli, H., and Peter, T.: Tropical troposphere-to-stratosphere transport inferred from trajectory calculations, J. Geophys. Res., 109, D03108, doi:10.1029/2003JD004069, 2004.

Giannakaki, E., Balis, D. S., Amiridis, V., and Kazadzis, S.: Optical and geometrical characteristics of cirrus clouds over a Southern European lidar station, Atmos. Chem. Phys., 7, 5519–5530, doi:10.5194/acp-7-5519-2007, 2007.

Goldfarb, L., Keckhut, P., Chanin, M.-L., and Hauchecorne, A.: Cirrus climatological results from lidar measurements at OHP (44° N, 6° E), Geophys. Res. Lett., 28, 1687–1690, doi:10.1029/2000GL012701, 2001.

Hallett, J., Arnott, W. P., Bailey, M. P., and Hallett, J. T.: Ice crystals in cirrus, edited by: Cirrus, edited by: Lynch, D. K., Sassen, K., Starr, D. O., and Stephens, G. L., 41–77, Oxford University Press, 2002.

Heymsfield, A. J.: Ice crystal terminal velocities, J. Atmos. Sci., 29, 1348–1357, doi:10.1175/1520-0469(1972)029<1348:ICTV>2.0.CO;2, 1972.

Heymsfield, A. J. and McFarquhar, G. M.: Mid-latitude and tropical cirrus, in: Cirrus, edited by: Lynch, D. K., Sassen, K., Starr, D. O'C., and Stephens, G., Oxford University Press, London, 78–101, 2002.

AMTD
6, 4087–4121, 2013

Heymsfield, A. J. and Platt, C. M. R.: A parameterization of the particle size spectrum of ice clouds in terms of the ambient temperature and the ice water content, J. Atmos. Sci., 41, 846–855, 1984.

Hoareau, C., Keckhut, P., Sarkissian, A., Baray, J.-L., and Durry, G.: Methodology for Water Monitoring in theUpperTroposphere with Raman Lidar at the Haute-Provence Observatory, J. Atmos. Ocean. Tech., 26, 2149–2160, 2009.

Hoareau, C., Keckhut, P., Baray, J.-L., Robert, L., Courcoux, Y., Porteneuve, J., Vömel, H., and Morel, B.: A Raman lidar at La Reunion (20.8° S, 55.5° E) for monitoring water vapour and cirrus distributions in the subtropical upper troposphere: preliminary analyses and description of a future system, Atmos. Meas. Tech., 5, 1333–1348, doi:10.5194/amt-5-1333-2012, 2012.

Josset, D., Pelon, J., Garnier, A., Hu, Y., Vaughan, M., Zhai, P.-W., Kuehn, R., and Lucker, P.: Cirrus optical depth and lidar ratio retrieval from combined CALIPSO-CloudSat observations using ocean surface echo, J. Geophys. Res., 117, D05207, doi:10.1029/2011JD016959, 2012.

Keckhut, P.: Rayleigh temperature lidar applications: Tools and methods, J. Phys. IV France, 139, 337–360, doi:10.1051/jp4:2006139022, 2006.

Keckhut, P., Hauchecorne, A., Bekki, S., Colette, A., David, C., and Jumelet, J.: Indications of thin cirrus clouds in the stratosphere at mid-latitudes, Atmos. Chem. Phys., 5, 3407–3414, doi:10.5194/acp-5-3407-2005, 2005.

Keckhut, P., Borchi, F., Bekki, S., Hauchecorne, A., and Silaouina, M.: Cirrus classification at mid-latitude from systematic lidar observations, J. Appl. Meteor. Clim., 45, 249–258, doi:10.1175/JAM2348.1, 2006.

Lampert, A.: Airborne Lidar Observations of Tropospheric Arctic Clouds, 2010 Thesis – Institute of Aerospace Systems, Technische Universität Carolo-Wilhelminazu Braunschweig, Germany, 2010.

Landulfo, E., Papayannis, A., Artaxo, P., Castanho, A. D. A., de Freitas, A. Z., Souza, R. F., Vieira Junior, N. D., Jorge, M. P. M. P., Sánchez-Ccoyllo, O. R., and Moreira, D. S.: Synergetic measurements of aerosols over São Paulo, Brazil using LIDAR, sunphotometer and satellite data during the dry season, Atmos. Chem. Phys., 3, 1523–1539, doi:10.5194/acp-3-1523-2003, 2003.

Lanzante, J. R.: Resistant, robust and non-parametric techniques for the analysis of climate data: Theory and examples, including applications to historical radiosonde station data, Int. J. Climatol., 16, 1197–1226, 1996.

AMTD
6, 4087–4121, 2013

Liou, K. N.: The Influence of Cirrus on Weather and Climate Process: A Global Perspective, Mon. Weather Rev., 114, 1167–1199, doi:10.1175/1520-0493(1986)114<1167:IOCCOW>2.0.CO;2, 1986.

Li, J.-L., Waliser, D. E., Jiang, J. H., Wu, D. L., Read, W., Waters, J. W., Tompkins, A., Donner, L. J., Chern, J.-D., Tao, W.-K., Atlas, R., Gu, Y., Liou, K. N., Del Genio, A., Khairoutdinov, M., and Gettelman, A.: Comparisons of EOS MLS cloud ice measurements with ECMWF analyses and GCM simulations: Initial Results, Geophys. Res. Lett., 32, L18710, doi:10.1029/2005GL023788, 2005.

Mioche, G., Josset, D., Gayet, J.-F., Pelon, J., Garnier, A., Minikin, A., and Schwarzenboeck, A.: Validation of the CALIPSO/CALIOP extinction coefficients from in situ observations in mid-latitude cirrus clouds during CIRCLE-2 experiment, J. Geophys. Res., 115, D00H25, doi:10.1029/2009JD012376, 2010.

Mitrescu, C.: Lidar model with parameterized multiple scattering for retrieving cloud optical properties, J. Quant. Spectrosc. Ra., 94, 201–224, doi:10.1016/j.jqsrt.2004.10.006, 2005.

Montoux, N., Keckhut, P., Hauchecorne, A., Jumelet, J., Brogniez, H., and David, C.: Isentropic modeling of a cirrus cloud event observed in the mid latitude upper troposphere and lower stratosphere, J. Geophys. Res., 115, D02202, doi:10.1029/2009JD011981, 2009.

Morille, Y., Haeffelin, M., Drobinski, P., and Pelon, J.: STRAT: An Automated Algorithm to Retrieve theVertical Structure of the Atmospherefrom Single-Channel Lidar Data, J. Atmos. Ocean. Tech., 24, 761–775, doi:10.1175/JTECH2008.1, 2007.

Nazaryan, H., McCormick, M. P., and Menzel, W. P.: Global characterization of cirrus clouds using CALIPSO data, J. Geophys. Res., 113, D16211, doi:10.1029/2007JD009481, 2008.

Platt, C. M. R.: Lidar and radiometric observations of cirrus clouds, J. Atmos. Sci., 30, 1191–1204, doi:10.1175/1520-0469(1973)030<1191:LAROOC>2.0.CO;2, 1973.

Platt, C. M. R., Young, S. A., Austin, R. T., Patterson, G. R., Mitchell, D. L., and Miller, S. D.: LIRAD observations of tropical cirrus clouds in MCTEX. Part I: Optical properties and detection of small particles in cold cirrus, J. Atmos. Sci., 59, 3145–3162, doi:10.1175/1520-0469(2002)059<3145:LOOTCC>2.0.CO;2, 2002.

Petty, D., Comstock, J., and Tuner, D.: Cirrus Extinction and Lidar Ratio Derived from Raman Lidar Measurements at the Atmospheric Radiation Measurement Program Southern Site, in: Proceedings of the Thirteenth Atmospheric Radiation Measurement Science TeamMeeting, Albuquerque, NM, 2006.

AMTD
6, 4087–4121, 2013

Ramanathan, V. and Collins, W.: Thermodynamics regulation of ocean warming by cirrus clouds deduced from observations of the 1987 El-Niño, Nature, 351, 27–32, doi:10.1038/351027a0, 1991.

Ringer, M. A. and Allan, R. P.: Evaluating climate model simulations of tropical cloud, Tellus A, 56, 308–327, doi:10.1111/j.1600-0870.2004.00061.x, 2004.

Sassen, K.: Cirrus Clouds – A modern perspective, in: Cirrus, edited by: Lynch, D. K., Sassen, K., Starr, D. O'C., and Stephens, G., Oxford University Press, London, 11–40, 2002.

Sassen, K. and Benson, S.: A mid-latitude cirrus cloud climatology from the facility for atmospheric remote sensing: Part II. Microphysical Properties Derived from Lidar Depolarization, Am. Meteorol. Soc., 58, 2103–2112, doi:10.1175/1520-0469(2001)058<2103:AMCCCF>2.0.CO;2, 2001.

Sassen, K. and Campbell, J. R.: A mid-latitude cirrus cloud climatology from the facility for atmospheric remote sensing: Part I. Macrophysical and synoptic properties, Am. Meteorol. Soc., 58, 481–496, doi:10.1175/1520-0469(2001)058<0481:AMCCCF>2.0.CO;2, 2001.

Sassen, K. and Cho, B.: Thin Cirrus Lidar Dataset for Satellite Verification and Climatological Research, Am. Meteorol. Soc., 31, 1275–1285, doi:10.1175/1520-0450(1992)031<1275:STCLDF>2.0.CO;2, 1992.

Sassen, K. and Comstock, J. M.: A Midlatitude Cirrus Cloud Climatology from the Facility for Atmospheric Remote Sensing. Part III: Radiative Properties, Am. Meteorol. Soc., 58, 2113–2127, doi:10.1175/1520-0469(2001)058<2113:AMCCCF>2.0.CO;2, 2001.

Sassen, K., Griffin, M., and Dood, G. C.: Optical scattering and microphysical properties of subvisible cirrus clouds, and climatic implications, J. Appl. Meteorol., 28, 91–98, doi:10.1175/1520-0450(1989)028<0091:OSAMPO>2.0.CO;2, 1989.

Sassen, K., Zhu, J., and Benson, S.: Mid-latitude Cirrus Cloud Climatology from the Facility for Atmospheric Remote Sensing. IV Optical displays: Radiative Properties, Appl. Optics, 42, 332–341, doi:10.1364/AO.42.000332, 2003.

Sassen, K., Wang, L., Starr, D. O'C., Comstock, J. M., and Quante, M.: A Midlatitude Cirrus Cloud Climatology from the Facility for Atmospheric Remote Sensing. Part V: Cloud Structural Properties, J. Atmos. Sci., 64, 2483–2501, doi:10.1175/JAS3949.1, 2007.

Sassen, K., Wang, Z., and Liu, D.: Global distribution of cirrus clouds from CloudSat/Cloud-Aerosol Lidar and Infrared Pathfinder Satellite Observations (CALIPSO) measurements, J. Geophys. Res., 113, D00A12, doi:10.1029/2008JD009972, 2008.

AMTD
6, 4087–4121, 2013

Seifert, P., Ansmann, A., Müller, D., Wandinger, U., Althausen, D., Heymsfield, A. J., Massie, S. T., and Schmitt, C.: Cirrus optical properties observed with lidar, radiosonde, and satellite over the tropical Indian ocean during the aerosol-polluted northeast and clean maritime southwest monsoon, J. Geophys. Res., 112, D17205, doi:10.1029/2006JD008352, 2007.

Takano, Y. and Liou, K. N.: Radiative transfer in cirrus clouds. III. Light scattering by irregular ice crystals, J. Atmos. Sci., 52, 818–837, doi:10.1175/1520-0469(1995)052<0818:RTICCP>2.0.CO;2, 1995.

Young, S. A.: Analysis of lidar backscatter profiles in optically thin clouds, Appl. Optics, 34, 7019–7031, doi:10.1364/AO.34.007019, 1995.

Wang, P. H., Minnis, P., McCormick, M. P., Kent, G. S., and Skeens, K. M.: A 6-year climatology of cloud occurrence frequency from Stratospheric Aerosol and Gas Experiment II observations (1985–1990), J. Geophys. Res., 101, 29407–29429, doi:10.1029/96JD01780, 1996.

Whiteman, D. N., Demoz, B., and Wang, Z.: Subtropical cirrus cloud extinction to backscatter ratios measured by Raman Lidar during CAMEX-3, Geophys. Res. Lett., 31, L12105, doi:10.1029/2004GL020003, 2004.

Winker, D. M., Powell, K., Trepte, C., Vaughan, M. A., and Wielicki, M. A.: The CALIPSO mission: A global 3D view of aerosols and clouds, B. Am. Meteorol. Soc., 91, 1211–1229, doi:10.1175/2010BAMS3009.1, 2010.

AMTD

6, 4087–4121, 2013

Towards an automatic Lidar cirrus cloud retrieval for climate studies

E. G. Larroza et al.

Table 1. Macro-physical properties of cirrus observed over São Paulo city on 11 June 2007.

Periods	z_{base} (km)	z_{top} (km)	z_{med} (km)	T_{zbase} (°C)	T_{ztop} (°C)	T_{zmed} (°C)	CT (km)
Multi-layer cloud – First Layer							
1	8.05	9.47	8.76	−26.77	−37.76	−32.47	1.42
2	7.75	9.56	8.65	−24.08	−38.50	−31.58	1.81
3	7.69	9.40	8.54	−23.61	−37.17	−30.74	1.70
4	7.85	9.01	8.43	−25.02	−34.49	−29.92	1.15
Multi-layer cloud – Second Layer							
1	9.79	11.19	10.49	−40.52	−52.87	−46.66	1.4
2	9.84	11.12	10.48	−41.01	−52.24	−46.59	1.28
3	10.05	10.89	10.47	−42.99	−49.98	−46.56	0.84
4	10.09	11.01	10.49	−43.33	−51.15	−47.2	0.91
Mono-layer cloud							
5	7.51	10.76	9.13	−21.88	−48.91	−35.47	3.27
6	8.44	10.74	9.59	−30.09	−48.8	−39.17	2.32
7	8.73	10.83	9.77	−32.19	−49.39	−40.64	2.12

AMTD
6, 4087–4121, 2013

Table 2. Optical properties of cirrus observed over São Paulo city on 11 June 2007.

Periods	TT	τ_{cir_app}	τ_{cir_eff}	LR_{app} (sr)	LR_{eff} (sr)
		Multi-layer cloud – First Layer			
1	0.76 ± 0.03	0.14 ± 0.02	0.13 ± 0.02	28 ± 4	26 ± 4
2	0.65 ± 0.02	0.21 ± 0.01	0.19 ± 0.01	22 ± 1	19 ± 1
3	0.83 ± 0.03	0.09 ± 0.02	0.09 ± 0.02	25 ± 4	24 ± 4
4	0.84 ± 0.03	0.09 ± 0.02	0.08 ± 0.02	35 ± 5	33 ± 5
		Multi-layer cloud – Second Layer			
1	0.58 ± 0.04	0.28 ± 0.03	0.24 ± 0.03	37 ± 4	32 ± 4
2	0.5 ± 0.02	0.35 ± 0.02	0.29 ± 0.02	39 ± 3	32 ± 3
3	0.65 ± 0.02	0.22 ± 0.02	0.19 ± 0.02	38 ± 4	34 ± 4
4	0.76 ± 0.02	0.14 ± 0.02	0.13 ± 0.02	74 ± 13	69 ± 12
		Mono-layer cloud			
5	0.16 ± 0.01	0.92 ± 0.01	0.56 ± 0.01	20 ± 1	12 ± 1
6	0.34 ± 0.01	0.54 ± 0.01	0.41 ± 0.01	20 ± 2	15 ± 2
7	0.48 ± 0.01	0.37 ± 0.01	0.30 ± 0.01	19 ± 1	16 ± 1

AMTD
6, 4087–4121, 2013

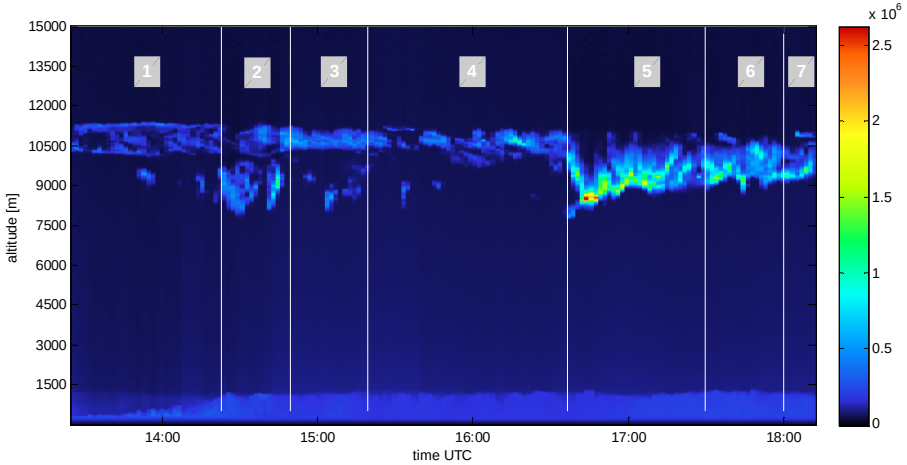

Fig. 1. A typical lidar-returned energy display of the troposphere on 11 June 2007, when cirrus clouds were observed by the MSP-lidar system (23°33′ S, 46°44′ W) over São Paulo City, Brazil. Note the aerosol backscattering layer up to 1 km, while the cirrus cloud is verified between 8.0 and 11.5 km.; The stationary periods are represented by seven periods (or observations, demonstrated also in Figs. 4 and 5) identified by the white vertical lines.

AMTD
6, 4087–4121, 2013

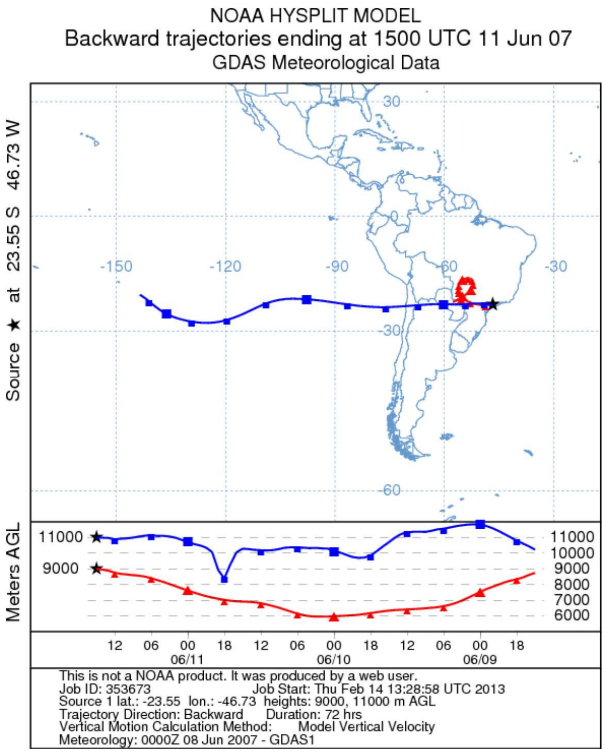

Fig. 2. NOAA HYSPLIT MODEL backward trajectories ending at 15:00 UTC on 11 June 2007 corresponding to the city of São Paulo (23°33′ S, 46°44′ W) showing the origin of air masses for the respective altitudes (∼ 9 km and 11 km) where cirrus clouds were detected by the MSP-lidar. The sequence of ending time was chosen on purpose to coincide with the period when two distinct cirrus layers were observed in Fig. 1, indicating here different origins.

AMTD
6, 4087–4121, 2013

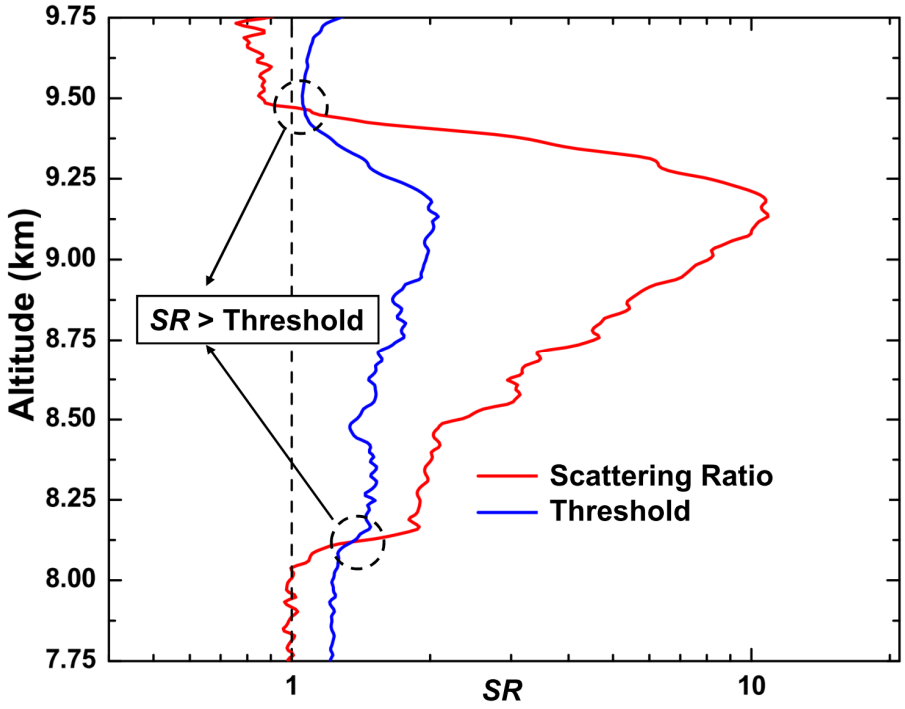

Fig. 3. Criterion to determine the base and top of cirrus clouds through threshold values.

AMTD
6, 4087–4121, 2013

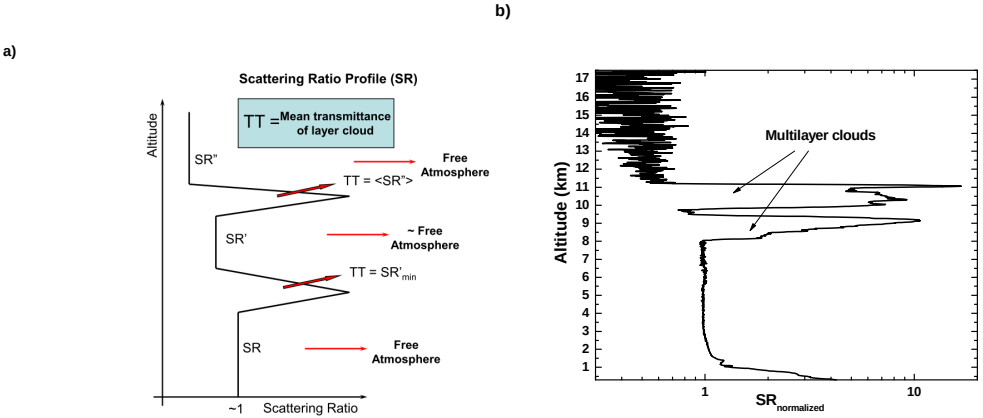

Fig. 4. (a) Criterion for obtaining the transmittance of cloud layers through SR'_{min} and $< SR'' >$ on the first and second cloud, respectively; **(b)** typical SR (normalized) signal profile. In both cases all profiles are actually apparent profiles.

AMTD
6, 4087–4121, 2013

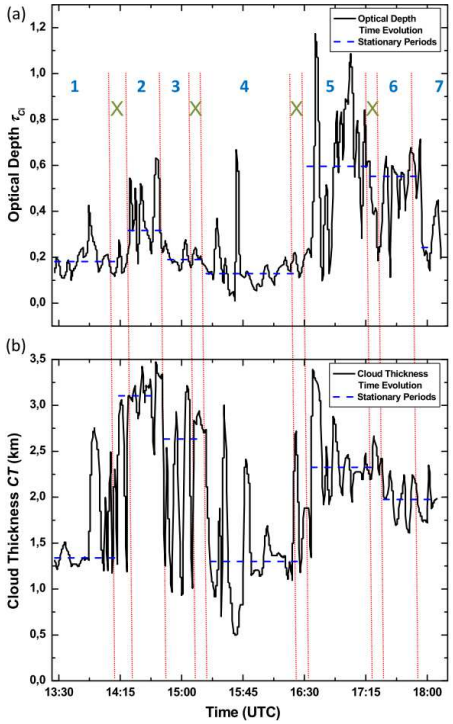

Fig. 5. Variation in time of: **(a)** Optical Depth (τ_{cir}) and **(b)** Cloud (Geometrical) Thickness (CT) for the altitude range between 8 and 11.5 km at São Paulo, Brazil from the MSP-lidar System. These variations are represented by the black solid line and the medians by the blue dashed lines, defining the stationary periods. Any contrary trend verified simultaneously between the τ_{cir} and CT values corresponding to the interval marked as green "X" were removed from the sequence.

AMTD
6, 4087–4121, 2013

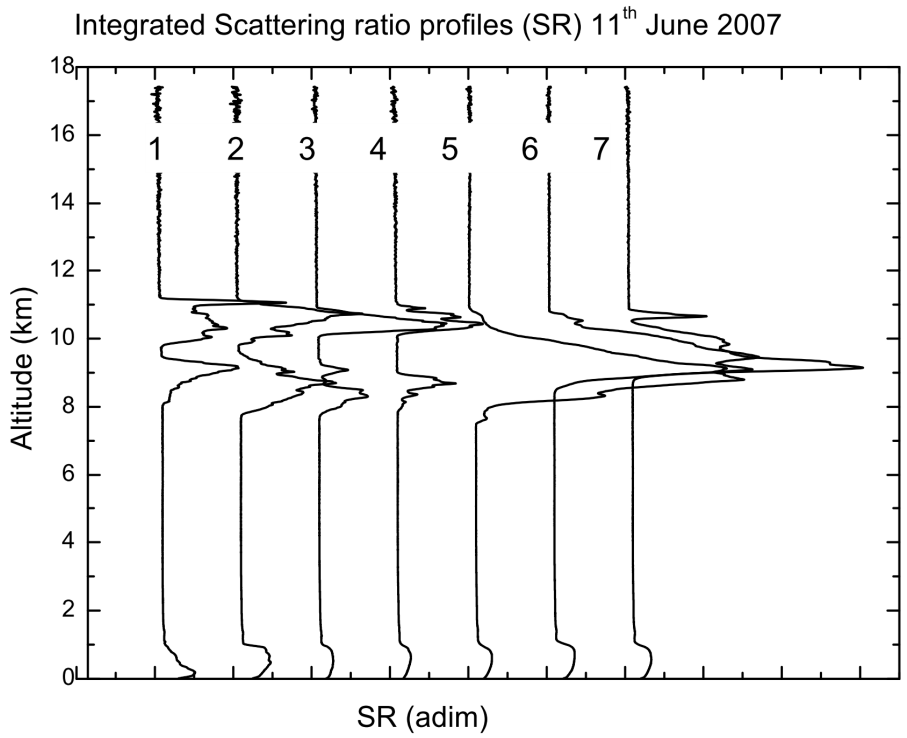

Fig. 6. Integrated Scattering Ratio (SR) profiles for 11 June 2007 corresponding to the respective stationary periods determined applying the statistical method suggested by Lanzante (1996). Is this case, seven independent profiles of SR were obtained.

AMTD
6, 4087–4121, 2013

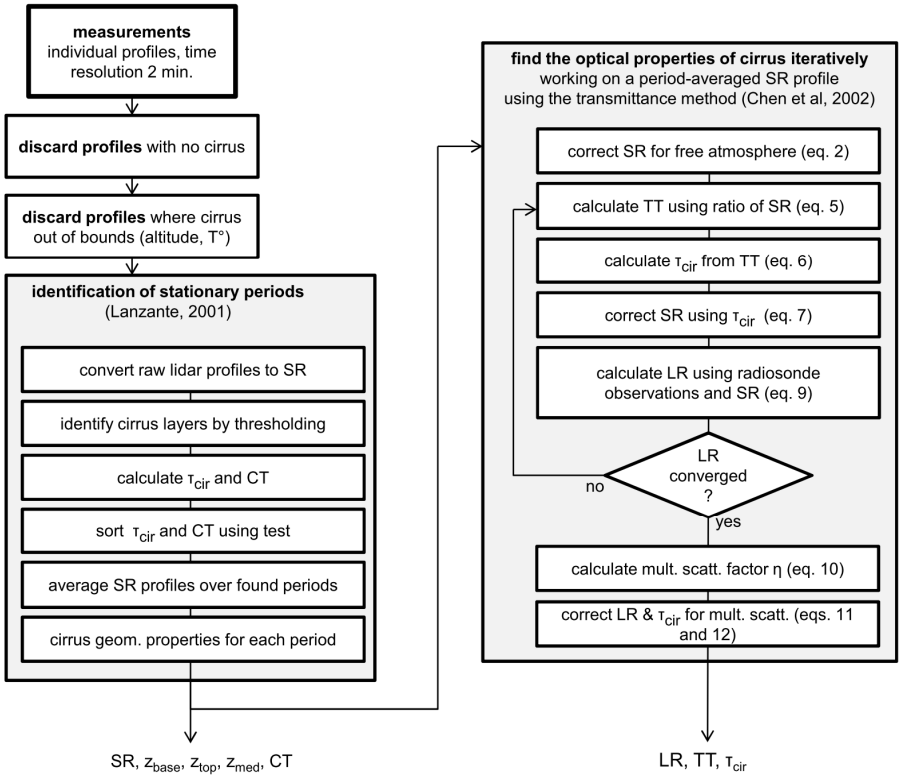

Fig. 7. Schematic flowchart showing the main steps of the methodology applied to obtain macro-physical and optical properties of cirrus clouds.

AMTD
6, 4087–4121, 2013

Towards an automatic Lidar cirrus cloud retrieval for climate studies

E. G. Larroza et al.